


 Cite this: *RSC Adv.*, 2020, 10, 42054

# Hot electron prompted highly efficient photocatalysis based on 3D graphene/non-precious metal nanoparticles†

 Suling Zhang,<sup>a</sup> Yanhong Lu,<sup>a</sup> \*<sup>a</sup> Xingchen Wan,<sup>a</sup> Yaxin Duan,<sup>a</sup> Junlin Gao,<sup>a</sup> Zhen Ge,<sup>b</sup> Lei Wei,<sup>a</sup> Yu Chen,<sup>a</sup> Yanfeng Ma<sup>\*b</sup> and Yongsheng Chen \*<sup>b</sup>

High dispersibility and rapid electron transfer are required for a highly efficient catalyst. In this work, such materials have been designed using a scalable hydrothermal method from graphene oxide and a metal-organic framework. A cross-linked three-dimensional graphene (3DGraphene) material loaded with mono-dispersed nitrogen-doped carbon-coated metallic Co (NC@Co) nanoparticles with uniform size of 12.2 nm (3DGraphene/NC@Co) has been obtained and exhibits excellent activity for catalytic reduction of 4-nitrophenol to 4-aminophenol. Such high catalytic activity can be assigned to the highly energetic hot/free electrons arising from 3DGraphene under light illumination and the synergistic effect between 3DGraphene and NC@Co nanoparticles. The catalytic reaction can be finished in 240 s with NaBH<sub>4</sub> as the reducing agent, and the corresponding rate constant (*k*) is  $1.5 \times 10^{-2} \text{ s}^{-1}$ , comparable to that of reported noble metal catalysts. Furthermore, the magnetic 3DGraphene/NC@Co materials are beneficial for the separation from the mixture after reaction and exhibit excellent cycling stability.

 Received 19th August 2020  
 Accepted 11th November 2020

DOI: 10.1039/d0ra07146c

[rsc.li/rsc-advances](http://rsc.li/rsc-advances)

## Introduction

Catalytic reduction of 4-nitrophenol (4-NP) to 4-aminophenol (4-AP) is considered as one of the most important reactions for the conversion of hazardous chemical materials. The design and preparation of catalysts with high activity have attracted considerable research interest.<sup>1–3</sup> Noble metal-based materials, such as Pt, Au and their composites are effective catalysts because of their high catalytic activity.<sup>4–7</sup> However, the limited supply, high cost of these noble metal-based catalysts severely hinders their widespread implementation in their applications. Development of low-cost and durable functional non-precious transition metals and/or their oxides based catalysts, such as Co/Co<sub>x</sub>O/Co<sub>x</sub>S<sub>y</sub>, Ni/NiO, Fe<sub>x</sub>O, *etc.*, with efficient catalytic activity, is thus highly demanded.<sup>8–11</sup>

The catalytic performance of a heterogeneous catalyst depends on its ability to bind with target molecules and facilitate electron transport or hydride transport for the reduction reactions.<sup>1</sup> Thus, it is critical to rationally design catalysts with

abundant active centers, depending on the smaller size, high dispersibility and stability, as well as the desired high electron transport ability of the catalysts.<sup>12,13</sup> Coating a layer of carbon materials on the metal nanoparticles surface has become a promising method to obtain smaller and highly dispersive catalyst nanoparticles.<sup>14,15</sup> Owing to their high specific surface area, excellent electronic conductivity and structural flexibility, porous carbons have been widely explored.<sup>10,16</sup> Metal-organic frameworks (MOFs), with metal moieties and organic linkers, are also promising precursors for building porous carbons coated metal nanoparticles through carbonization.<sup>14,17</sup> With their high exposure of the active sites and the fast rate of mass transfer, these MOFs derived metal-porous carbon hybrids have shown improved catalytic activities.<sup>18,19</sup> However, the metal atoms in MOFs may aggregate easily during high temperature pyrolysis process, and the relatively low electronic conductivity also limits their catalytic activities.<sup>20</sup> A facile method to prevent the aggregation of the nanoparticles and at the same time to improve the conductivity is to grow MOFs on conductive carbon materials, and there have been tremendous studies about two-dimensional (2D) graphene sheets as support materials for MOFs.<sup>21–23</sup> However, the intrinsic and robust intention of restacking of 2D graphene sheets due to their strong  $\pi$ - $\pi$  interaction between the sheets severely limit the efficient exposure of all the open metal-based active sites.

Monolithic three-dimensional (3D) cross-linked graphene (3DGraphene) bulk materials have attracted increasing interest as a support to load catalyst nanoparticles.<sup>24,25</sup> Such these composites could not only preserve the small size, high

<sup>a</sup>School of Chemistry & Material Science, Langfang Normal University, Langfang, 065000, China. E-mail: [luyanhong@lfnu.edu.cn](mailto:luyanhong@lfnu.edu.cn); Fax: +86-316-218-8376; Tel: +86-316-218-8376

<sup>b</sup>The Centre of Nanoscale Science and Technology, Key Laboratory of Functional Polymer Materials, State Key Laboratory and Institute of Elemento-Organic Chemistry, College of Chemistry, Nankai University, Tianjin, 300071, China. E-mail: [yanfengma@nankai.edu.cn](mailto:yanfengma@nankai.edu.cn); [yschen99@nankai.edu.cn](mailto:yschen99@nankai.edu.cn); Fax: +86-22-2350-0693; Tel: +86-22-2350-0693

† Electronic supplementary information (ESI) available. See DOI: 10.1039/d0ra07146c



dispersibility and exposure of the active catalytic sites, but also possess suitable pore networks. Simultaneously, the multidimensional electron transport path-ways deliver an extraordinary electronic transport property in catalytic reactions.<sup>20,26,27</sup> More importantly, 3DGraphene materials have an unique property of emitting hot/free electrons under light illumination, which could exhibit highly efficient catalytic properties.<sup>28–30</sup> Furthermore, with magnetic nanoparticles, the 3DGraphene based composites can be easily recycled, which is imperative to the development of high-performance catalysts for cost-effective industrial process.

In the previous works, 3DGraphene loaded metal/metal oxide particles using as catalysts for the reduction of 4-NP were studied. The preparation procedures include template<sup>31</sup> or hydrothermal<sup>32,33</sup> methods using the corresponding metal salt as the precursors. These preparation processes have severe limitations for highly active catalyst, including the inferior dispersibility, insufficient size controlling, and more importantly, defective 3DGraphene structures abandoned the excellent intrinsic properties.

Herein, using a designed structure of cobalt-based zeolitic imidazolate framework-67 (ZIF-67) as an effective precursor and template, 3DGraphene loaded porous nitrogen-doped carbon-coated cobalt nanoparticles (3DGraphene/NC@Co) were prepared. ZIF-67, composed of cobalt nodes and 2-methylimidazole ligands, can be converted to porous carbon with an abundance of Co–N–C active sites.<sup>22</sup> Thus, 3DGraphene/NC@Co possess highly exposed active sites and an extraordinary properties, which arise from the synergistic effect between 3DGraphene and the nitrogen-doped carbon-coated cobalt nanoparticles (NC@Co). This composite catalyst exhibits high catalytic activity and efficiency toward catalytic reduction of 4-NP to 4-AP, with a completed reduction time of 240 s and a corresponding high rate constant ( $k$ ) of  $1.5 \times 10^{-2} \text{ s}^{-1}$ , comparable to the widely used noble metal catalysts.

## Experimental section

### Material synthesis

All chemicals used in this work are analytical grade and used directly without further treatment unless otherwise noted. Deionized (DI) water was used in all experiments. Graphene oxide (GO) was synthesized by the oxidation of natural graphite powder using a modified Hummers' method according to our previous procedures.<sup>24,28</sup>

**Synthesis of ZIF-67.** Cobaltous nitrate hexahydrate ( $\text{Co}(\text{NO}_3)_2 \cdot 6\text{H}_2\text{O}$ , 1 mmol, 291 mg) and 2-methylimidazole (4 mmol, 328 mg) were first dissolved in 25 mL of methanol, respectively. Then, the solution of 2-methylimidazole was quickly added into the solution of cobaltous nitrate, and the resultant mixed solution was kept ageing for 24 h at room temperature.<sup>34</sup> The resulting ZIF-67 crystals with purple color were collected by centrifugation, washed with methanol for several times, and then dried in a vacuum oven at 70 °C for 6 h.

**Synthesis of 3DGraphene/ZIF-67.** The 3DGraphene supported ZIF-67 composites were prepared through a solvothermal process. Typically, the prepared ZIF-67 crystals

(120 mg) was added to a GO ethanol dispersion (30 mL, 1.0 mg  $\text{mL}^{-1}$ ) and stirred for 30 min to mix uniformly. The mixture was then sealed in a 50 mL Teflon-lined autoclave, heated to 180 °C and maintained for 12 h. After the autoclave was cooled to the room temperature, the ethanol-filled products were carefully transferred to a beaker and had a slow and gradually solvent exchange with water. The water wholly filled products were freeze-dried and then dried in a vacuum oven at 120 °C for 12 h.

**Synthesis of 3DGraphene/NC@Co.** The previous 3DGraphene/ZIF-67 composites were annealed at 600 °C for 2 h in Ar to obtain the final 3DGraphene loaded porous nitrogen-doped carbon frameworks embedded with cobalt nanoparticle material.

As control catalysts to compare, 3DGraphene and ZIF-67 were also annealed at the same conditions as that for 3DGraphene/NC@Co, and the final samples were named as 3DGraphene-annealing and ZIF-67-annealing, respectively. They were also tested for their catalytic activity for comparison.

### Characterization

The structures of the samples were investigated by X-ray diffraction (XRD) performed on a Rigaku D/Max-2500 diffractometer with Cu  $K\alpha$  radiation. Raman spectrum was performed with a Renishaw InVia Raman spectrometer using laser excitation at 514.5 nm. Lorentzian fitting was carried out to confirm the positions and widths of the D and G bands.  $I_D$  and  $I_G$  are the intensities of the D and G bands, respectively. X-ray photoelectron spectroscopy (XPS) analysis was performed using AXIS HIS 165 spectrometer (Kratos Analytical) with a monochromatized Al  $K\alpha$  X-ray source (1486.7 eV). Scanning electron microscopy (SEM) images were obtained on an FEI NanoSem 430 field emission scanning electron microscope using an accelerating voltage of 20 kV. Transmission electron microscopy (TEM) and high-resolution transmission electron microscopy (HR-TEM) were conducted in an FEI Tecnai G2 F20 electron microscope using an acceleration voltage of 200 kV.

### Catalytic reduction of 4-nitrophenol

The catalytic reduction process was carried out under ambient conditions, and the light comes from the sunlight and the excitation light of the UV-vis spectra. Typically,  $\text{NaBH}_4$  (1.0 mL, 0.25 M), 4-nitrophenol (1.0 mL, 0.5 mM) and DI water (1.0 mL) were mixed in a colorimeter cell. Then, an aqueous suspension of 3DGraphene/NC@Co (0.1 mL, 0.5 mg  $\text{mL}^{-1}$ ) was added to the solution. After adding the catalyst, the color of the 4-NP and  $\text{NaBH}_4$  solution gradually faded from yellow-green to colorless with the reaction proceeded. The reduction process of 4-NP to 4-AP was monitored by recording the UV-vis spectra at short intervals in the range of 250–500 nm. With the change in the spectral intensity at  $\lambda = 400 \text{ nm}$  as a function of time, the rate constants ( $k$ ) for the catalytic reduction of 4-NP was examined.<sup>35</sup> The rate constants of the catalytic reaction at 0, 15, 25 and 35 °C were studied. Based on the series of rate constants, the activation energy ( $E_a$ ) was calculated according to the Arrhenius equation.



For comparison, the catalytic activity of the control catalysts, ZIF-67-annealing and 3DGraphene-annealing were also investigated under the same condition. At the same time, the control reaction without any catalyst under the same conditions was also carried out.

## Results and discussion

### Design and synthesis of 3DGraphene/NC@Co

As discussed above, to obtain the catalysts with high activity, it is critical to achieve the active metal nanoparticles with smaller size as well as high dispersibility. This requires not only proper design of the support structure but also precise control of the morphology of the active metal particles. Here, ZIF-67 crystals (Fig. S1, ESI†) are chosen as the precursor of NC@Co to control the dispersion of metal particles during the inVia construction of 3DGraphene with GO as the precursor using a solvothermal process. The schematic synthesis process of 3DGraphene/NC@Co is illustrated in Scheme 1. During this solvothermal process, the 3DGraphene network can be constructed *via* the covalent cross-linking of the functional groups such as OH, COOH, and epoxy groups mainly located on the GO sheets edges.<sup>24,25</sup> Simultaneously, the dispersed ZIF-67 crystals are spontaneously self-assembled on the surface of GO sheets through the non-covalent bond, such as hydrogen bonding between the H atoms of ZIF-67 and the -OH/-COOH of graphene sheets. The following freeze-drying process can keep the cross-linked 3D porous structure of the composites. The final carbonization process under Ar can not only convert the ZIF-67 crystals to nitrogen-doped carbon-coated cobalt nanoparticles, but also partly reduce GO to graphene. Thus, the 3DGraphene loaded porous nitrogen-doped carbon-coated cobalt nanoparticles will be prepared.

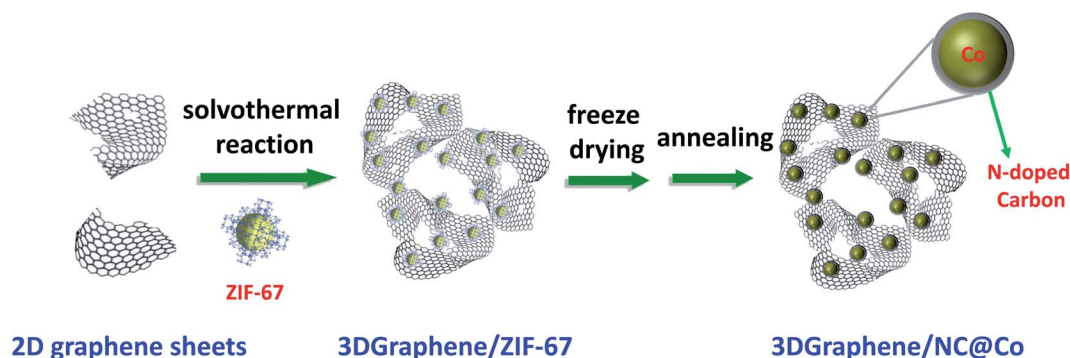
### Structure and morphology characterization

The morphologies of the prepared 3DGraphene/NC@Co composite are shown in Fig. 1. The SEM images (Fig. 1a and b) exhibit the cross-linked 3DGraphene skeleton structures, originated from the efficient assembly of the wrinkled GO sheets during the hydrothermal process,<sup>24,25</sup> which is beneficial for the formation of highly dispersed cobalt nanoparticles. As

shown in the high magnified SEM image (Fig. 1b), the catalyst particles are uniformly dispersed on the surface of GO sheets in the interconnected 3D structures. TEM is further employed to evaluate the nanostructures of the 3DGraphene/NC@Co composite. Fig. 1c shows the catalyst nanoparticles, with an average diameter of about 12.2 nm (inset of Fig. 1c), are uniformly dispersed on the graphene network, which agrees well with the SEM results. In the HR-TEM, as shown in Fig. 1d, cobalt nanoparticles encapsulated in carbon skeletons are clearly observed. Notably, the carbon shell is derived from the annealing of ZIF-67 under high temperature.

The structural properties of 3DGraphene/NC@Co composites were further investigated using XRD and Raman analysis. As shown in Fig. 2a, all the diffraction peaks in the XRD patterns of the prepared ZIF-67 in the  $2\theta$  range of 5–30° match well with the reported results.<sup>21,36</sup> In the XRD pattern of 3DGraphene/NC@Co composite, the broad peak at 26.2° corresponds to the (002) diffraction of the graphene material. The peak at 44° is indexed to the (111) crystal plane of face-centered (fcc) Co (PDF#15-0806),<sup>18</sup> indicating that ZIF-67 deposited on 3DGraphene has been partially transformed into metallic Co. The more structure characteristic of cobalt and the disordered structure of 3DGraphene can also be supported by the Raman spectrum. In Fig. 2b, the D band for the disordered carbon crystallites at 1356 and G band for crystalline graphite at 1592  $\text{cm}^{-1}$  are shown. The large value of the full width at half maximum of D and G bands (~144.2 and 68.4, respectively) and the high ratio of integrated intensities of D and G bands ( $I_D/I_G = 2.10$ ) demonstrate a high degree of structural disorder of 3DGraphene. Such highly disordered structures could provide abundant active sites for accelerating charge transfer rate and stabilizing the nanoparticles.<sup>37</sup> The characteristic peak at 675  $\text{cm}^{-1}$  can be observed, corresponding to the existence of cobalt oxide.<sup>38</sup> The XRD result, combined with Raman analysis, show that the metal nanoparticles derived from ZIF-67 on 3DGraphene consist of metallic cobalt and cobalt oxide. It is noted that, in the XRD result, due to the hump of carbon, the peaks of cobalt oxide is not noticeable.

XPS analysis is usually employed to confirm the surface composition and chemical state of the catalysts. The XPS survey spectrum of 3DGraphene/NC@Co composite (Fig. 3a) reveals the presence of C, O, N, and Co in the composites and the



Scheme 1 Schematic illustration of the preparation process of 3DGraphene/NC@Co composite.



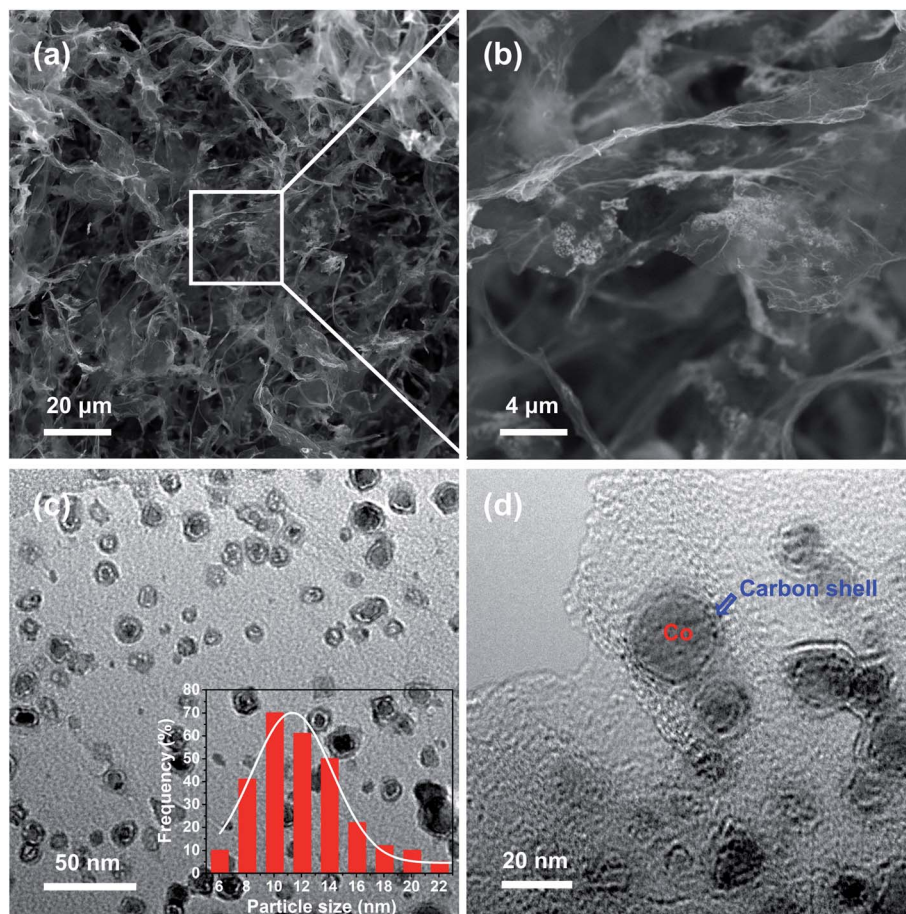


Fig. 1 The morphologies of 3DGraphene/NC@Co. (a and b) SEM, (c) TEM and (d) HR-TEM images. Inset in (c) is the statistical diameter distribution charts of ~280 particles.

atomic ratio is 86.84%, 10.28%, 0.79% and 2.09%, respectively. The high-resolution C 1s spectrum (Fig. 3b) is deconvoluted into  $sp^2$  carbon (284.2 eV), C–N (285.8 eV), and C–O (287.9 eV).<sup>14</sup> The presence of the C–N bond confirms the successful doping of N in the process of ZIF-67 forming the carbon layer. The corresponding high-resolution XPS spectrum of N 1s (Fig. 3c) shows the existence of two types of N configuration, Co–N, and

graphitic-N at the binding energies of 399.2 and 401.2 eV, respectively.<sup>17,37</sup> The high-resolution spectrum of Co 2p, as shown in Fig. 3d, reveals the peaks corresponding to metallic Co at 779.5 and 794.5 eV,<sup>39–41</sup> Co–N–C at 780.7 eV and Co–N species at 796.2 eV.<sup>14</sup> The satellite band at 784.5 eV come from the cobalt oxide.<sup>21</sup> The XPS analyses display the coexistence of metallic cobalt and cobalt oxide, corresponding to the XRD and

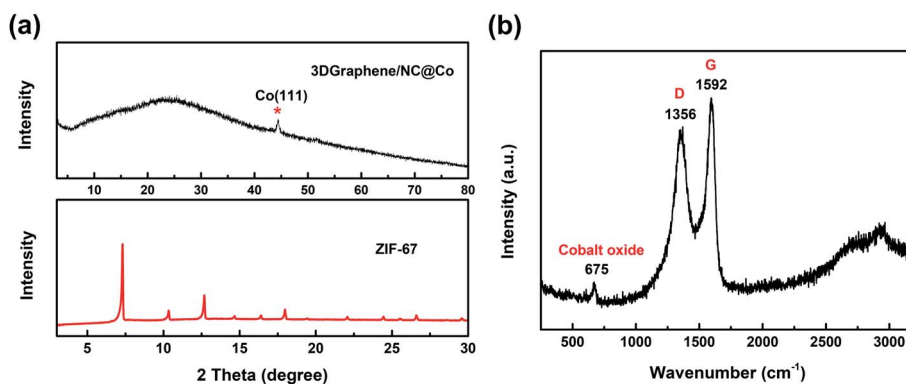


Fig. 2 Structure analysis of prepared materials. (a) XRD results of ZIF-67 and 3DGraphene/NC@Co. (b) Raman spectrum of 3DGraphene/NC@Co.



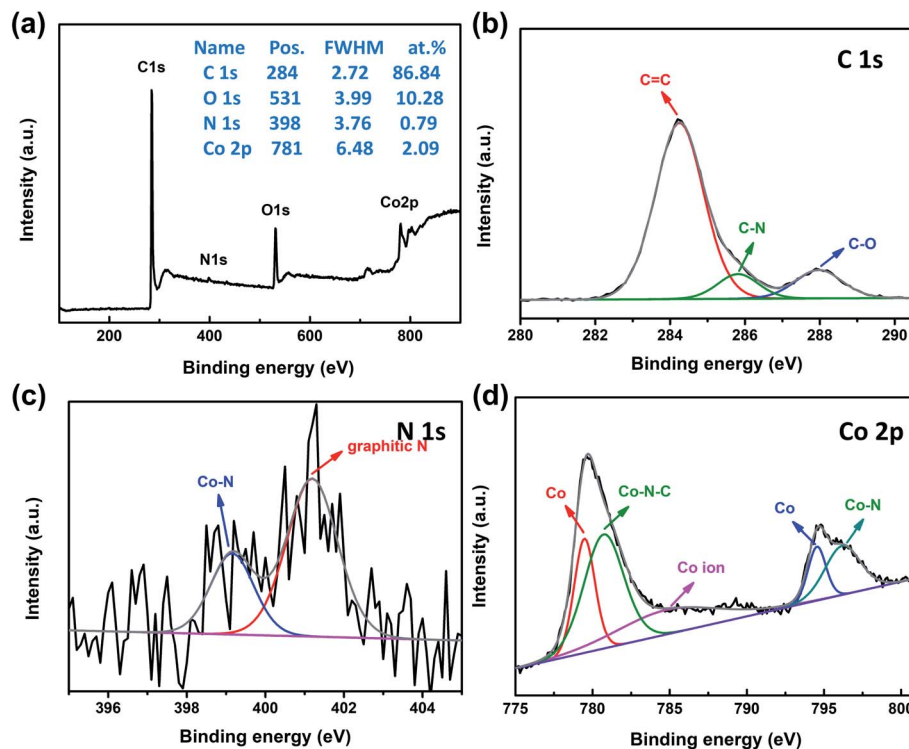


Fig. 3 XPS spectra of 3DGraphene/NC@Co. (a) Survey spectrum, and high-resolution spectra of (b) C 1s, (c) N 1s, and (d) Co 2p.

Raman results. Notably, the existence of Co-N-C and Co-N species indicates the presence of M-N-C bonds, which can be highly active toward catalysis reaction.<sup>14</sup>

### Catalytic activity for the reduction of 4-nitrophenol

The catalytic activity of 3DGraphene/NC@Co composite and the control samples (ZIF-67-annealing and 3DGraphene-annealing, prepared under the same conditions) were evaluated using the reduction reaction of 4-NP to 4-AP as a model system. The 4-NP solution shows a strong absorption peak at 317 nm under neutral or acidic conditions. After addition of NaBH<sub>4</sub> solution, the absorption peak of 4-NP changed from 317 to 400 nm immediately (Fig. S2, ESI<sup>†</sup>), correspondingly, the color changed from light yellow to yellow-green due to the formation of the 4-nitrophenolate ion in basic medium.<sup>4</sup> With the addition of the 3DGraphene/NC@Co catalyst, the color of the 4-nitrophenolate ions gradually faded away and became colorless finally. Meanwhile, the absorbance at  $\lambda_{\max} = 400$  nm decreased, and a new peak emerged at  $\lambda_{\max} = 300$  nm, corresponding to the formation of 4-AP. Notably, without any catalyst, the reaction rate of reduction of 4-NP by NaBH<sub>4</sub> was relatively slow, which can be reflected from the negligible decrease of the absorption peak at  $\lambda_{\max} = 400$  nm over a period of time (Fig. S3, ESI<sup>†</sup>). Fig. 4 demonstrates the catalytic activities of 3DGraphene/NC@Co and the control catalysts of ZIF-67-annealing and 3DGraphene-annealing for the reduction reaction of 4-NP to 4-AP. 3DGraphene/NC@Co shows the best and significantly enhanced catalytic activity, which lead to the solution completely colorless in 240 s (Fig. 4a), indicating a complete

reduction of 4-NP to 4-AP. As a contrast, the retention of the corresponding absorbance of ZIF-67-annealing and 3DGraphene-annealing is 43% and 94% at 240 s (Fig. 4b and c), respectively. Based on above comparison and analyses, the much enhanced catalytic activities of the 3DGraphene/NC@Co could be attributed to the excellent structure and charge transfer ability of the composites.

Consider that the catalytic reaction follows the pseudo-first-order kinetics with respect to the concentration of 4-NP with excess NaBH<sub>4</sub>, the apparent rate constant ( $k$ ) can be calculated followed the kinetic equation given as:<sup>1,42</sup>

$$\ln C_t/C_0 = -kt$$

where,  $C_0$  and  $C_t$  are the initial concentration ( $t = 0$ ) of 4-NP and that at time  $t$ , respectively. The data of  $\ln(C_t/C_0)$  versus time ( $t$ ) were linearly fitted, and the slope of the plots was the rate constant ( $k$ ). The rate activity parameter ( $k'$ ) of the rate constant normalized with the mass of catalyst used in the reaction was also calculated. Among the series of catalysts, 3DGraphene/NC@Co materials exhibit the maximum rate constant  $k$  of  $1.5 \times 10^{-2} \text{ s}^{-1}$  and  $k'$  of  $3.0 \times 10^{-1} \text{ s}^{-1} \text{ mg}^{-1}$ , which are more than twice of that of ZIF-67-annealing (Fig. 4d and e). Note that the rate constant for 3DGraphene/NC@Co is higher than the sum of ZIF-67-annealing and 3DGraphene-annealing under the same conditions. These results indicate that there must be some synergistic effect for this composite catalyst, and this will be discussed later. Furthermore, the rate constant obtained in this study is by far much higher than several noble/non-precious metal/metal oxide catalysts, as shown in Table 1.



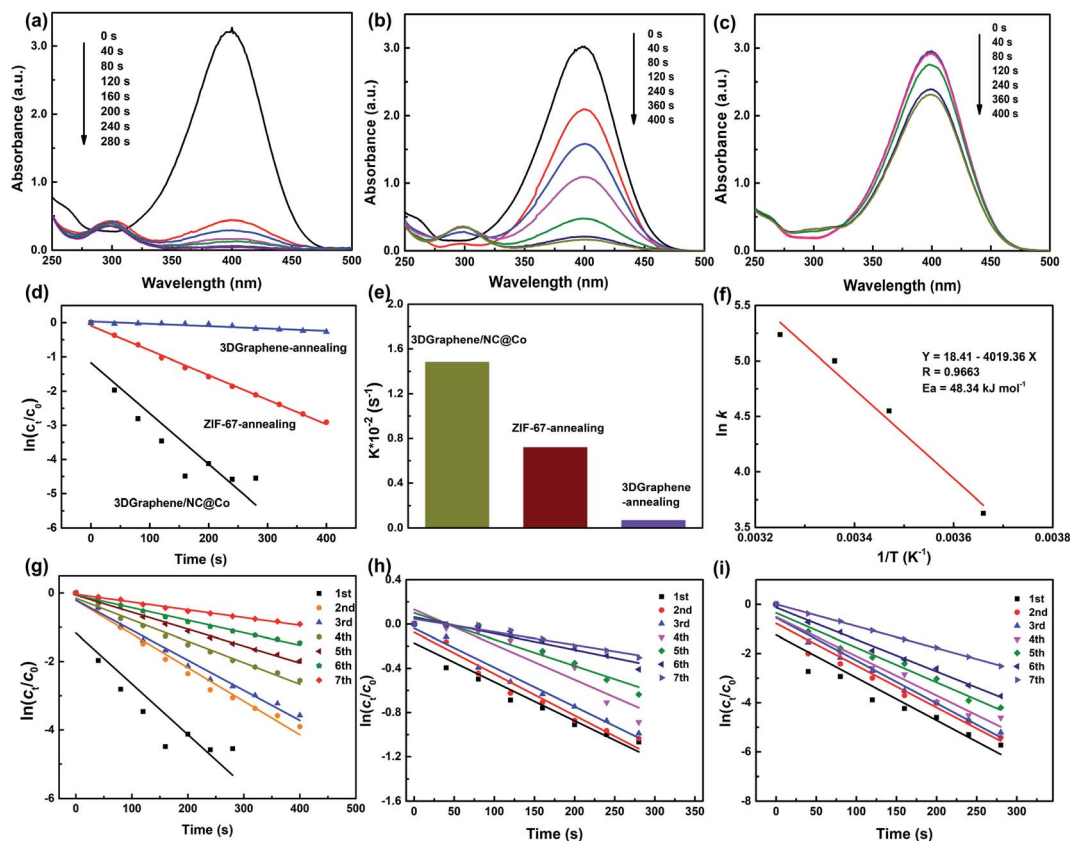


Fig. 4 Catalytic activity of 3DGraphene/NC@Co and the control catalysts. (a–c) Successive UV-vis spectra for the reduction reaction of 4-NP by NaBH<sub>4</sub> with catalysts of (a) 3DGraphene/NC@Co, (b) ZIF-67-annealing and (c) 3DGraphene-annealing. (d) The plot of  $\ln(C_t/C_0)$  versus time  $t$  and (e) the comparison of the rate constants for the reduction of 4-NP with the three kinds of catalysts. (f) The fitting line of  $\ln k$  versus  $1/T$ . (g–i) Cycling stabilities of 3DGraphene/NC@Co catalyst for the reduction of 4-NP at 25, 0 and 35 °C, respectively.

Table 1 Comparison of rate constants  $k$  and activity parameter  $k'$  of 3DGraphene/NC@Co with the reported catalysts for the reduction of 4-NP to 4-AP

Catalyst	$k \times 10^{-3}$ (s <sup>-1</sup> )	$k' \times 10^{-3}$ (s <sup>-1</sup> mg <sup>-1</sup> )	Ref.
FeCo-NCNS/TRGO-0.050	4.00	0.80	9
Ni/rGO@Au	8.73	97.0	43
AuNRs/GO	28.2	8.56	12
CoFe <sub>2</sub> O <sub>4</sub> -2.0	340	34.0	44
3DG@CS@AuNSs	6.33	—	31
Ru/H <sub>x</sub> MoO <sub>3-y</sub> (100)	1.05	—	45
Au/PEI/GO	9.87	1.97	46
CuO-MnO <sub>2</sub> NPs	5.20	5.20	47
Au/g-C <sub>3</sub> N <sub>4</sub>	7.90	7.90	48
CuO nanorods	6.70	6.70	32
Au/CoFe <sub>2</sub> O <sub>4</sub>	5.4	—	49
3DGraphene/NC@Co	15.0	300	This work

To further study the catalytic performance of 3DGraphene/NC@Co catalyst for the reduction of 4-NP, the thermodynamic parameter of activation energy  $E_a$  were investigated by carrying out the reaction at 0, 15, 25 and 35 °C respectively. The

apparent rate constants at each temperature was obtained. Then the activation energy was calculated using the Arrhenius equation, as shown in Fig. 4f. The low  $E_a$  of 48.34 kJ mol<sup>-1</sup>, similar to the data reported in the literature,<sup>8</sup> demonstrate the high activities of 3DGraphene/NC@Co catalyst.

The cycling stability and reusability is a critical feature for the evaluation of heterogeneous catalyst. Thus, 3DGraphene/NC@Co catalyst was recycled and used in a new reaction to test the catalytic activity for seven cycles and the corresponding rate constants testing at 0, 25 and 35 °C are shown in Fig. 4g–i. The detailed rate constants for each cycle of catalytic reaction at different temperature are exhibited in Tables S1–S3 (ESI†). For the series of cycling experiments, the  $k$  value decreases slightly after each cycle, indicating a good recycling ability of 3DGraphene/NC@Co catalyst at each temperature in the range of 0–35 °C. Notably, due to the magnetic characteristics of the 3DGraphene/NC@Co catalyst, it can be recycled easily from the solution, which is another critical issue in practical applications.

### Catalytic mechanism

Based on the results above, especially for the 3DGraphene/NC@Co material, noticeable catalytic activity was observed. The much enhanced catalytic activity of the composite should



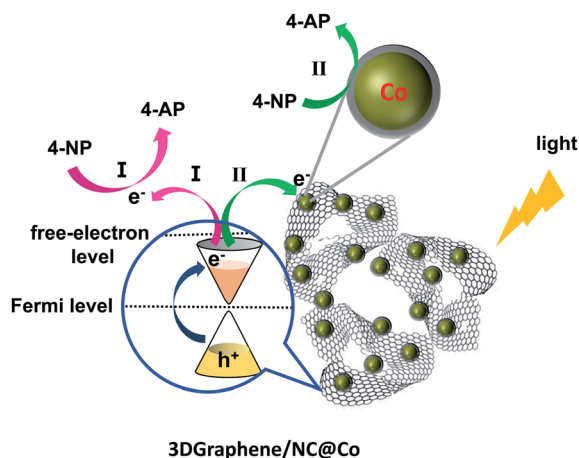


Fig. 5 The reaction mechanism of photocatalytic reduction of 4-NP to 4-AP with 3DGraphene/NC@Co catalyst.

contribute to the synergistic catalytic effect from 3DGraphene<sup>30</sup> and the embedded cobalt nanoparticles.<sup>1,10</sup> As observed before,<sup>28–30</sup> 3DGraphene itself can efficiently generate a high density of hot/free electrons under full-spectrum (including UV, visible and IR) light illumination, and such highly energetic hot/free electrons can be ejected from 3DGraphene into free space *via* an Auger-like mechanism. These hot/free electrons, behaving as massless Dirac fermions, can act as powerful reducing agents for driving the initial photo-reduction reaction. Thus, under the illumination of visible light and the UV-vis light from the ultraviolet spectrometer, the catalytic process of 3DGraphene/NC@Co composite for reduction of 4-NP to 4-AP in this study can be envisaged that it performs through two pathways, as illustrated in Fig. 5. In one way (path I), 3DGraphene in the composite can work as a bare photocatalyst itself, where highly energetic hot/free electrons generated under illumination could effectively reduce the 4-NP molecules directly adsorbed on the surface of the graphene sheets. In the other way (path II), on the contact surface of graphene sheets and cobalt nanoparticles, due to a lower work function of 3DGraphene than that of cobalt, the hot/free electrons ejected from 3DGraphene under light illumination can quickly and efficiently transfer to metallic cobalt, resulting in an electron-enriched region surrounding the cobalt nanoparticles. These highly energetic hot/free electrons can significantly facilitate the reduction reaction of the 4-NP molecules assembled near the active cobalt centers.<sup>4</sup> Thus, these electron transfer *via* hot/free electron mechanisms would cause a higher catalytic activity than that of the sum of individual ZIF-67-annealing and 3DGraphene-annealing (Fig. 4e), indicating a synergistic effect between 3DGraphene and the cobalt nanoparticles.

## Conclusions

In summary, a novel composite catalyst with nano Co particles embedded in 3DGraphene has been constructed through a simple solvothermal reaction. With a hot/free electron mechanism and the synergistic effect between 3DGraphene and

the embedded cobalt nanoparticles, 3DGraphene/NC@Co exhibits excellent and much enhanced catalytic activity and cycling stability for the reduction of 4-NP to 4-AP by NaBH<sub>4</sub> in an aqueous solution. The reduction conversion of 4-NP can achieve nearly 100% within 240 s, and the corresponding rate constant  $k$  can reach  $1.5 \times 10^{-2} \text{ s}^{-1}$ . For the cycling stability, after seven successive recycles of the catalyst, it still retains significant conversion efficiencies, even at 0 and 35 °C. Moreover, the freestanding cross-linked 3DGraphene bulk material could improve the catalyst's performance in separation and reuse. This work might provide some guidelines to develop novel non-precious metal catalyst through a facile, environment-friendly approach.

## Conflicts of interest

There are no conflicts of interest to declare.

## Acknowledgements

The authors gratefully acknowledge the financial support from the National Natural Science Foundation of China (NSFC, 51502125), the Natural Science Foundation of Hebei Province of China (Grant E2020408004, B2017408042, E2016408035), Hebei Talent Engineering Training Support Project (A201901064), Key Laboratory of Functional Polymer Materials (Nankai University) of Ministry of Education, the Excellent Going Abroad Experts Training Program in Hebei Province, the Fundamental Research Funds for the Universities in Hebei Province (JYT201901, JYQ201902), the Research Project of Hebei Education Department of China (BJ2016044), the Doctor Fund of Langfang Normal University (LSLB201401) and the Hebei Higher Education Teaching Reform Research and Practice Project (2019GJJG357).

## References

- 1 A. Sharma, R. K. Dutta, A. Roychowdhury, D. Das, A. Goyal and A. Kapoor, *Appl. Catal., A*, 2017, **543**, 257–265.
- 2 M. Ma, Y. Yang, W. Li, R. Feng, Z. Li, P. Lyu and Y. Ma, *J. Mater. Sci.*, 2019, **54**, 323–334.
- 3 U. Alam, S. Kumar, D. Bahnemann, J. Koch, C. Tegenkamp and M. Muneer, *Phys. Chem. Chem. Phys.*, 2018, **20**, 4538–4545.
- 4 P. Zhang, C. Shao, X. Li, M. Zhang, X. Zhang, C. Su, N. Lu, K. Wang and Y. Liu, *Phys. Chem. Chem. Phys.*, 2013, **15**, 10453–10458.
- 5 W. Zhang, G. Lu, C. Cui, Y. Liu, S. Li, W. Yan, C. Xing, Y. R. Chi, Y. Yang and F. Huo, *Adv. Mater.*, 2014, **26**, 4056–4060.
- 6 X. Liu, Q. Han, Y. Zhang, X. Wang, S. Cai, C. Wang and R. Yang, *Appl. Surf. Sci.*, 2019, **471**, 929–934.
- 7 W. Gong, Q. Wu, G. Jiang and G. Li, *J. Mater. Chem. A*, 2019, **7**, 13449–13454.
- 8 B. M. Mogudi, P. Ncube and R. Meijboom, *Appl. Catal., B*, 2016, **198**, 74–82.



- 9 L. Ma, X. Shen, G. Zhu, Z. Ji and H. Zhou, *Carbon*, 2014, **77**, 255–265.
- 10 X. Li, C. Zeng, J. Jiang and L. Ai, *J. Mater. Chem. A*, 2016, **4**, 7476–7482.
- 11 R. M. Zhou, X. Y. Yang, P. Zhang, L. X. Yang, C. W. Liu, D. Liu and J. Z. Gui, *Phys. Chem. Chem. Phys.*, 2018, **20**, 27730–27734.
- 12 J. Fang, X. Chen, Y. Wu and H. Liu, *J. Mater. Sci.*, 2020, **55**, 5880–5891.
- 13 S. Mansingh, R. Acharya, S. Martha and K. M. Parida, *Phys. Chem. Chem. Phys.*, 2018, **20**, 9872–9885.
- 14 S. G. Peera, J. Balamurugan, N. H. Kim and J. H. Lee, *Small*, 2018, **14**, 1800441.
- 15 B. N. Bhadra, N. A. Khan and S. H. Jhung, *J. Mater. Chem. A*, 2019, **7**, 17823–17833.
- 16 N. L. Torad, M. Hu, S. Ishihara, H. Sukegawa, A. A. Belik, M. Imura, K. Ariga, Y. Sakka and Y. Yamauchi, *Small*, 2014, **10**, 2096–2107.
- 17 L. Chen, Y. Li, N. Xu and G. Zhang, *Carbon*, 2018, **132**, 172–180.
- 18 F. Yang, P. Zhao, X. Hua, W. Luo, G. Cheng, W. Xing and S. Chen, *J. Mater. Chem. A*, 2016, **4**, 16057–16063.
- 19 Y. Yusran, D. Xu, Q. Fang, D. Zhang and S. Qiu, *Microporous Mesoporous Mater.*, 2017, **241**, 346–354.
- 20 W. Xia, C. Qu, Z. Liang, B. Zhao, S. Dai, B. Qiu, Y. Jiao, Q. Zhang, X. Huang, W. Guo, D. Dang, R. Zou, D. Xia, Q. Xu and M. Liu, *Nano Lett.*, 2017, **17**, 2788–2795.
- 21 X. Bai, J. Liu, Q. Liu, R. Chen, X. Jing, B. Li and J. Wang, *Chem.–Eur. J.*, 2017, **23**, 14839–14847.
- 22 J. Wei, Y. Hu, Y. Liang, B. Kong, Z. Zheng, J. Zhang, S. P. Jiang, Y. Zhao and H. Wang, *J. Mater. Chem. A*, 2017, **5**, 10182–10189.
- 23 Y. Wang, X. Gao, C. Lin, L. Shi, X. Li and G. Wu, *J. Alloys Compd.*, 2019, **785**, 765–773.
- 24 Y. Wu, N. Yi, L. Huang, T. Zhang, S. Fang, H. Chang, N. Li, J. Oh, J. A. Lee and M. Kozlov, *Nat. Commun.*, 2015, **6**, 6141.
- 25 Y. Lu, Y. Ma, T. Zhang, Y. Yang, L. Wei and Y. Chen, *J. Am. Chem. Soc.*, 2018, **140**, 11538–11550.
- 26 B. Wang, L. Si, J. Geng, Y. Su, Y. Li, X. Yan and L. Chen, *Appl. Catal., B*, 2017, **204**, 316–323.
- 27 D. Sui, L. Xu, H. Zhang, Z. Sun, B. Kan, Y. Ma and Y. Chen, *Carbon*, 2020, **157**, 656–662.
- 28 T. Zhang, H. Chang, Y. Wu, P. Xiao, N. Yi, Y. Lu, Y. Ma, Y. Huang, K. Zhao, X.-Q. Yan, Z.-B. Liu, J.-G. Tian and Y. Chen, *Nat. Photonics*, 2015, **9**, 471–476.
- 29 Y. Lu, Y. Yang, T. Zhang, Z. Ge, H. Chang, P. Xiao, Y. Xie, L. Hua, Q. Li, H. Li, B. Ma, N. Guan, Y. Ma and Y. Chen, *ACS Nano*, 2016, **10**, 10507–10515.
- 30 Y. Lu, B. Ma, Y. Yang, E. Huang, Z. Ge, T. Zhang, S. Zhang, L. Li, N. Guan, Y. Ma and Y. Chen, *Nano Res.*, 2017, **10**, 1662–1672.
- 31 Z. Ma, Y. Qiu, Y. Huang, F. Gao and P. Hu, *RSC Adv.*, 2015, **5**, 79456–79462.
- 32 A. Bhattacharjee and M. Ahmaruzzaman, *RSC Adv.*, 2016, **6**, 41348–41363.
- 33 J. Li, C.-y. Liu and Y. Liu, *J. Mater. Chem.*, 2012, **22**, 8426–8430.
- 34 H. Hu, B. Guan, B. Xia and X. W. Lou, *J. Am. Chem. Soc.*, 2015, **137**, 5590–5595.
- 35 K. Cui, W. Zhong, L. Li, Z. Zhuang, L. Li, J. Bi and Y. Yu, *Small*, 2019, **15**, 1804419.
- 36 R. B. Wu, X. K. Qian, X. H. Rui, H. Liu, B. L. Yadian, K. Zhou, J. Wei, Q. Y. Yan, X. Q. Feng, Y. Long, L. Y. Wang and Y. Z. Huang, *Small*, 2014, **10**, 1932–1938.
- 37 M. Zhang, Q. Dai, H. Zheng, M. Chen and L. Dai, *Adv. Mater.*, 2018, **30**, 1705431.
- 38 K.-Y. A. Lin, F.-K. Hsu and W.-D. Lee, *J. Mater. Chem. A*, 2015, **3**, 9480–9490.
- 39 X. Lu, Y. Liu, Y. He, A. N. Kuhn, P.-C. Shih, C.-J. Sun, X. Wen, C. Shi and H. Yang, *ACS Appl. Mater. Interfaces*, 2019, **11**, 27717–27726.
- 40 Y. J. Oh, J. H. Kim and Y. C. Kang, *Chem. Eng. J.*, 2019, **373**, 86–94.
- 41 X. F. Lu, Y. Chen, S. Wang, S. Gao and X. W. Lou, *Adv. Mater.*, 2019, **31**, 1902339.
- 42 J. Wu, W. Liu, X. Xiang, K. Sun, F. Liu, C. Cai, S. Han, Y. Xie, S. Li and X. Zu, *Carbon*, 2017, **117**, 192–200.
- 43 M. Cao, L. Feng, P. Yang, H. Wang, X. Liang and X. Chen, *J. Mater. Sci.*, 2018, **53**, 4874–4883.
- 44 J.-L. Ortiz-Quinonez and U. Pal, *ACS Omega*, 2019, **4**, 10129–10139.
- 45 H. Yin, Y. Kuwahara, K. Mori, M. Che and H. Yamashita, *J. Mater. Chem. A*, 2019, **7**, 3783–3789.
- 46 M. Zhang, X. Lu, H.-Y. Wang, X. Liu, Y. Qin, P. Zhang and Z.-X. Guo, *RSC Adv.*, 2016, **6**, 35945–35951.
- 47 J. Pal, C. Mondal, A. K. Sasmal, M. Ganguly, Y. Negishi and T. Pal, *ACS Appl. Mater. Interfaces*, 2014, **6**, 9173–9184.
- 48 Y. Fu, T. Huang, B. Jia, J. Zhu and X. Wang, *Appl. Catal., B*, 2017, **202**, 430–437.
- 49 S. Saire-Saire, E. C. M. Barbosa, D. Garcia, L. H. Andrade, S. Garcia-Segura, P. H. C. Camargo and H. Alarcon, *RSC Adv.*, 2019, **9**, 22116–22123.

